Journal of Medicinal Chemistry

Article

pubs.acs.org/jmc

Catechol Pyrazolinones as Trypanocidals: Fragment-Based Design, Synthesis, and Pharmacological Evaluation of Nanomolar Inhibitors of Trypanosomal Phosphodiesterase B1

Kristina M. Orrling,[†] Chimed Jansen,[†] Xuan Lan Vu,[‡] Vreni Balmer,[§] Patrick Bregy,[‡,●] Anitha Shanmugham,[∥] Paul England,[∥] David Bailey,[∥] Paul Cos,[⊥] Louis Maes,[⊥] Emily Adams,[#] Erika van den Bogaart,[#] Eric Chatelain,[∞] Jean-Robert Ioset,[∞] Andrea van de Stolpe,[†] Stèphanie Zorg,[†] Johan Veerman,[×] Thomas Seebeck,[‡] Geert Jan Sterk,[×] Iwan J. P. de Esch,[†] and Rob Leurs*[,†]

[†]Leiden/Amsterdam Centre of Drug Research (LACDR), Amsterdam Institute of Molecules, Medicines and Systems (AIMMS), Division of Medicinal Chemistry, VU University Amsterdam, De Boelelaan 1083, 1081 HV Amsterdam, The Netherlands

[‡]Institute of Cell Biology, University of Bern, Baltzerstrasse 4, 3012 Bern, Switzerland

[§]Institute of Parasitology of the University of Bern, University of Bern, Baltzerstrasse 4, 3012 Bern, Switzerland

[∥]IOTA Pharmaceuticals, St. John's Innovation Centre, Cowley Road, Cambridge CB4 0WS, United Kingdom

[⊥]Laboratory for Microbiology, Parasitology and Hygiene (LMPH), University of Antwerp, Groenenborgerlaan 171, 2020 Wilrijk, Belgium

[#]Department of Biomedical Research, Royal Tropical Institute Amsterdam, Meibergdreef 39, 1105 AZ Amsterdam, The Netherlands

[∞]DND*i* (Drugs for Neglected Diseases *initiative*), 15 Chemin Louis Dunant, 1202 Geneva, Switzerland

[×]Mercachem, P.O. Box 6747, 6503 GE Nijmegen, The Netherlands

Supporting Information

ABSTRACT: Trypanosomal phosphodiesterases B1 and B2 (TbrPDEB1 and TbrPDEB2) play an important role in the life cycle of *Trypanosoma brucei*, the causative parasite of human African trypanosomiasis (HAT), also known as African sleeping sickness. We used homology modeling and docking studies to guide fragment growing into the parasite-specific P-pocket in the enzyme binding site. The resulting catechol pyrazolinones act as potent TbrPDEB1 inhibitors with IC_{50} values down to 49 nM. The compounds also block parasite proliferation (e.g., VUF13525 (**20b**): *T. brucei rhodesiense* IC_{50} = 60 nM, *T. brucei brucei* IC_{50} = 520 nM, *T. cruzi* = 7.6 μM), inducing a typical multiple nuclei and kinetoplast phenotype without being generally cytotoxic. The mode of action of **20b** was investigated with recombinantly engineered trypanosomes expressing a cAMP-sensitive FRET sensor, confirming a dose-response related increase of intracellular cAMP levels in trypanosomes. Our findings further validate the TbrPDEB family as antitrypanosomal target.

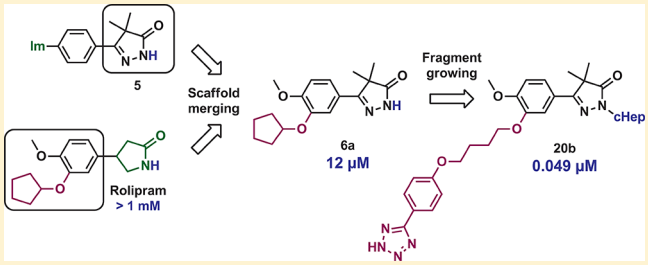

INTRODUCTION

Human African trypanosomiasis (HAT), commonly known as African sleeping sickness, is an extremely deadly disease; without treatment, all patients entering second stage HAT following the spread of the parasite to the CNS will eventually die.[1] Millions of people are living in the endemic areas in rural central Africa, where poverty and poor access to accurate healthcare hamper the chances of survival of infected patients.[2,3] Even if the number of reported cases has dropped to its lowest level in 50 years, epidemics, increased political turbulence, and resistance emergence can quickly alter this trend.[3,4] HAT is caused by the kinetoplastid protozoa *Trypanosoma brucei* and is transmitted by infected tsetse flies (*Glossina* ssp.). Two subspecies of *T. brucei* are infectious to humans, *T. b. gambiense* and *T. b. rhodesiense*. The course of the disease, symptoms, and appropriate treatment depend on the etiological subspecies.[2] Despite the high medical need, current treatment options are limited and suffer from suboptimal dosage regimens and/or severe toxicity.[2] During the second stage of the disease, the only choices are the arsenic-containing drug melarsoprol and the ornithine decarboxylase inhibitor eflornithine, used as monotherapy or in combination with nifurtimox (NECT).[5] However, eflornithine is not effective against *T. b. rhodesiense*. Consequently, public−private initiatives such as the Drugs for Neglected Disease *initiative* investigate new approaches to target HAT.[6]

Received: July 20, 2012
Published: September 10, 2012

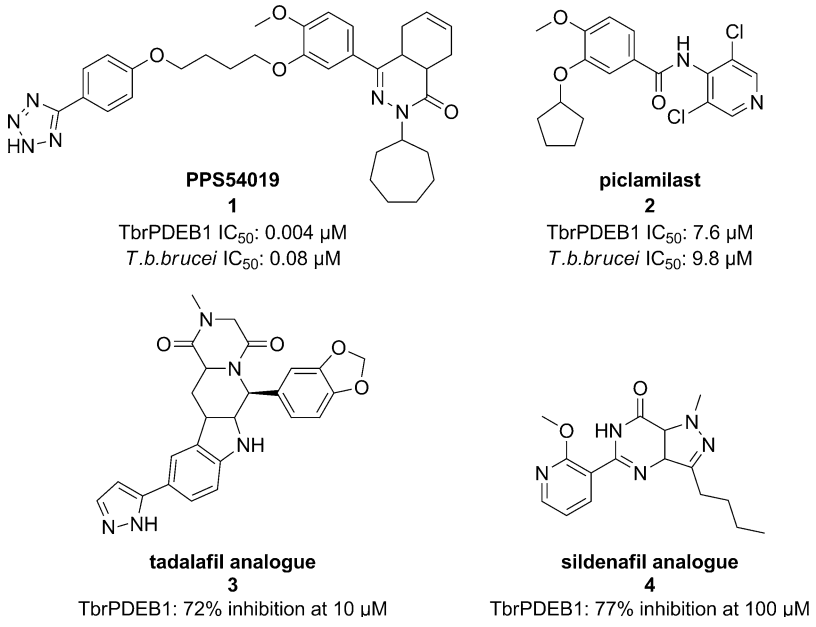

Figure 1. Known TbrPDE inhibitors **1**,[12] **2**,[14] **3**,[15] and **4**.[16]

The mapping of the *T. brucei* genome revealed the presence of five trypanosomal cyclic nucleotide phosphodiesterases (PDEs).[7] These enzymes play an important role in the regulation of cyclic nucleotide levels by catalyzing the hydrolysis of the phosphodiester bond of cAMP and/or cGMP. In humans, 11 main families of PDEs can be distinguished, and several of the human PDE enzymes have been extensively explored as molecular targets for a diverse set of diseases conditions, e.g., COPD, erectile dysfunction, pulmonary arterial hypertension, asthma, psoriasis, type 2 diabetes, depression, cognitive disorders, and psychosis. Although the exact role of cAMP in the life cycle of the trypanosomes is not fully understood,[8] two trypanosomal PDEs have been found to play a pivotal role in *T. brucei* proliferation.[9,10] Knocking down of both TbrPDEB1 and TbrPDEB2 simultaneously leads to an arrest of parasite cell division, lysis of the parasites, and elimination of the infection in vivo in the infected mouse model.[11] Additional studies on a hit from a high throughput screening campaign, PPS54019 (**1**), pharmacologically validated TbrPDEB1 and TbrPDEB2 as antitrypanosomal targets.[12] In fact, **1** was once synthesized as potent human PDE4 inhibitor.[13] The benefits of extracting acquired knowledge from very advanced drug discovery programs targeting human proteins for use in neglected diseases drug discovery cannot be overestimated. Scarcity in the drug research pipeline can thus be compensated with better pharmacological predictability and an early understanding of possible adverse effects. A recent investigation shows that the hPDE4 inhibitor piclamilast (**2**) and analogues also inhibit TbrPDEB1 and TbrPDEB2 (Figure 1).[12,14] Inhibition of TbrPDEB1 has furthermore been observed with analogues of tadalafil (**3**)[15] and sildenafil (**4**),[16] both hPDE5 inhibitors, however, at high micromolar concentrations.

These findings indicate that in the area of neglected infectious diseases, basing drug discovery efforts on lead compounds originally developed for human PDE targets can be quite a successful strategy. Such an approach proved to be successful in not only the discovery of the first TbrPDEB1 inhibitors **1**−**4** but also the recent discovery of antiplasmodial compounds based on the PDE5 inhibitor tadalafil.[17]

From a follow-up on chemotypes related to HTS hit **1**, catechol pyrazolinone **6a** (TbrPDEB1 inhibition with IC_{50} = 12 μM) was discovered. This fragment contains several structural features of known human PDE inhibitors and can be considered a product of merging the known PDE4 inhibitor rolipram (i.e., catechol moiety connected to a cyclopentyl group, also present in **2**) and of published cardiotonic hPDE3 inhibitors **5**[18,19] and hPDE4 inhibitors in the patent literature[20] (i.e., the pyrazolinone moiety) as outlined in Scheme 1.

Scheme 1. Design Idea Behind the Original TbrPDEB1 Inhibitor 6a, Where Rolipram Contributed the Catechol Moiety and 5[18,19] the Pyrazolinone Scaffold[a]

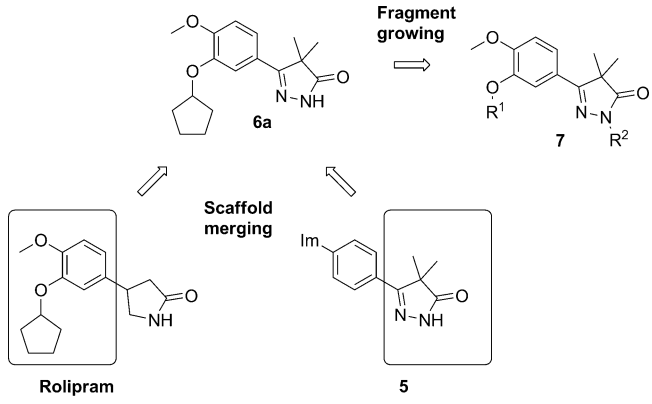

[a]The general structure of the herein reported TbrPDEB1 inhibitors is represented by **7**.

Following these fragment-based drug design considerations, we investigated the putative binding mode of these compounds by constructing a homology model of TbrPDEB1 based on the X-ray structure (PDB code 2R8Q)[21] of the *Leishmania major* orthologue LmjPDEB1 (66% sequence identity). Interestingly, the so-called P-pocket, a unique subpocket that extends from the invariant glutamine (Gln874) through the protein to the

dx.doi.org/10.1021/jm301059b | J. Med. Chem. 2012, 55, 8745−8756

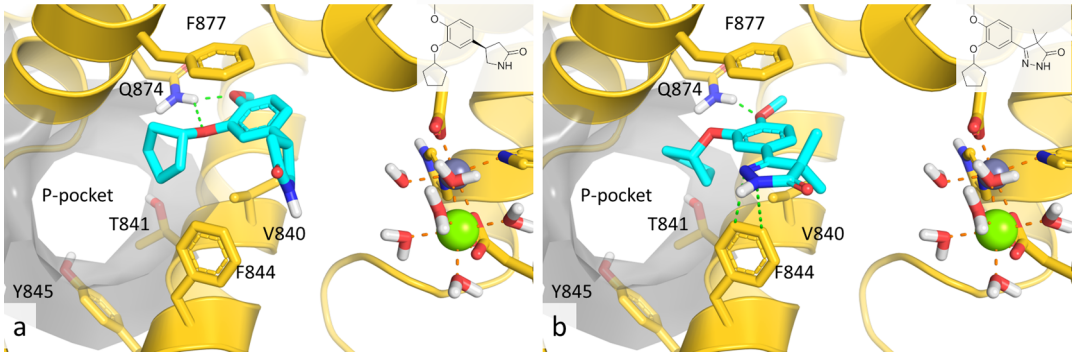

Figure 2. Proposed binding modes of (a) rolipram and (b) pyrazolinone **6a** in the TbrPDEB1 homology model. Both compounds interact with the highly conserved Gln874 and Phe877, and the cyclopentyl moiety is placed at the entrance of the P-pocket. (b) The pyrazolinone ring is involved in a $\pi-\pi$ interaction with Phe844.

Scheme 2. Synthetic Route to Pyrazolinones[a]

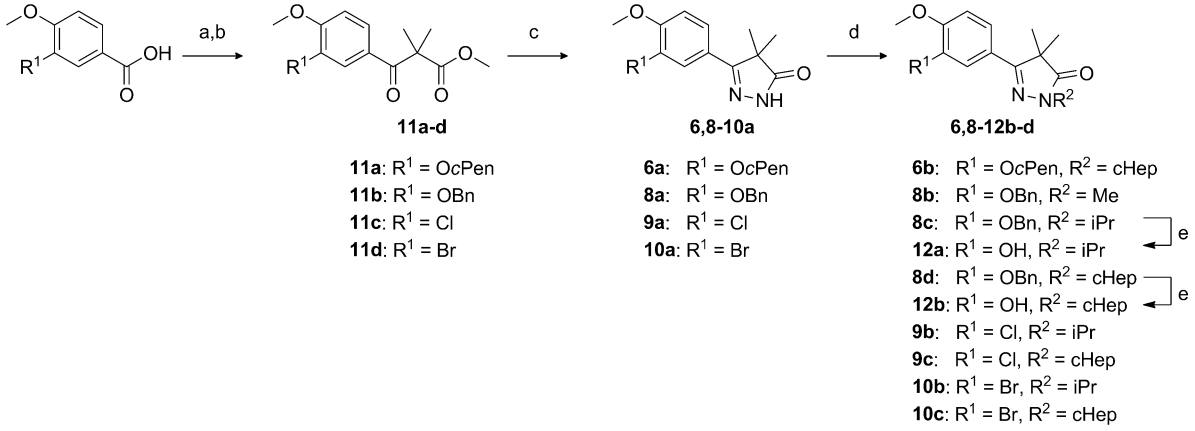

[a]Reagents: (a) $(COCl)_2$, DMF, CH_2Cl_2, 1−18 h or $SOCl_2$, rt, 1−2 h; (b) methyl isobutanoate, LDA, THF, −45 °C, 30 min, then added to acyl chloride, −55 °C to rt, 1−18 h; (c) N_2H_4, EtOH, reflux, 18 h. (d) **8b**: K_2CO_3, DMF, MW (145 °C, 20 min), then MeI, MW (145 °C, 20 min). **8c,d, 9−10b,c**: R^2Br, NaH, DMF/MeCN, MW (120 °C, 40 min). (e) Pd/C, NH_4CHO_2, MeOH/CH_2Cl_2 (2:1), 40 °C, 18 h.

solvent in the ligand-binding site of the LmjPDEB1, proved to be conserved in our model of TbrPDEB1.

Docking studies suggested rolipram to be well accommodated in the homology model of TbrPDEB1. The docked binding poses of rolipram identified the catechol motif as the main potential contributor of affinity to the protein, being well positioned in the hydrophobic clamp between Phe877 and Val840 and hydrogen bonding with Gln874, while the lactam ring was less well positioned, making no specific interactions (Figure 2a). However, biochemical measurements indicate rolipram to be inactive at >100 μM on the TbrPDEB1 enzyme.

A pyrazolinone is a heterocycle related to the lactam ring of rolipram but holds a conjugated π-system and additional possibility to interact with aromatic residues in the binding pocket (Figure 2b).

In this binding pose, the cyclopentyl ring of **6a** is placed at the entrance of the P-pocket, making this an interesting region to optimize, leading to compounds with the general structure **7** (Scheme 1). A second vector to be decorated was placed at the pyrazolinone nitrogen (R^2), in line with phthalazinone-based hPDE4 inhibitors.[22]

RESULTS AND DISCUSSION

Homology Model of TbrPDEB1. The homology model of TbrPDEB1 was constructed based on the TbrPDEB1 sequence published by Zoraghi and Seebeck (Uniprot code Q8WQX9)[9] and the structure of LmjPDB1 (2R8Q),[21] the only orthologue of TbrPDEB1 crystallized to date. The B chain of the LmjPDEB1 structure was used to construct the homology model, since the B factors in the region of the catalytic site are lower in the B chain. The residues on the surface of the catalytic site show a very high sequence homology with only one V836I substitution. The P-pocket region has two substitutions, N881M and R885K, both on the far side of the P-pocket from the invariant glutamine (Gln874). The overall sequence identity of the catalytic domains is 66%.

Synthetic Chemistry. The pyrazolinones **6**, **8−10a** were formed in good yields (67−99%) from a heterocyclization reaction with aqueous hydrazine and the corresponding β-ketoesters **11a−d**.[18,19] In contrast to previously reported synthetic routes, the β-ketoesters **11a−d** were synthesized from the corresponding benzoic acids via the benzoyl chloride and the enolate of methyl isobutyrate (Scheme 2). The ring nitrogen was alkylated using NaH and isopropyl bromide or cycloheptyl bromide and heated either by microwave (MW) irradiation or refluxing overnight, depending on the reaction scale, to give **8c,d** and **9−10b,c**. The methyl group in pyrazolinone **8b** was introduced in a similar fashion but using K_2CO_3 as base. In an attempt to reduce the number of reaction steps, cycloheptylhydrazine hydrogen chloride salt was used in the pyrazolinone-formation reaction, but this resulted in a complex reaction mixture and poor yield (17%) of required

dx.doi.org/10.1021/jm301059b | J. Med. Chem. 2012, 55, 8745−8756

Scheme 3. Synthetic Route to Catechol Pyrazolinones[a]

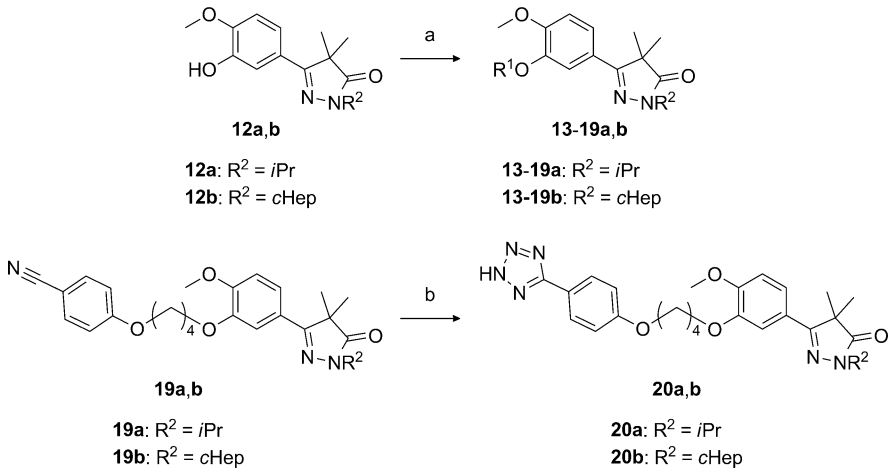

[a]Reagents. (a) Method A: R^1Br, K_2CO_3, DMF/MeCN, MW (120 °C, 30 min), then R^1Br or R^1Cl, MW (120 °C, 20–60 min). Method B: NaH, DMF, R^1Br, MW (120 °C, 15–30 min. (b) NaN_3, NH_4Cl, DMF, MW (160 °C, 1 h).

Table 1. Inhibitory Potency against TbrPDEB1, *T. b. brucei* Proliferation, and Cytotoxicity of Pyrazolinones

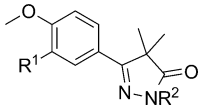

				IC_{50} (μM)		CC_{50} (μM)	
compd	R^1	R^2	yield (%)[a]	TbrPDEB1	*T. b. brucei*	MRC5	LE[c]
rolipram				>100	nt[b]	nt[b]	
6a	OcPen	H	15	12	>64	>64	0.30
6b	OcPen	*c*Hep	89	0.41	>64	>64	0.30
8a	OBn	H	97	6.3	8.6	55	0.30
8b	OBn	Me	98	10	32	>64	0.27
8c	OBn	*i*Pr	73	1.0	4.5	52	0.30
8d	OBn	*c*Hep	75	0.50	6.3	>64	0.28
12a	OH	*i*Pr	96	>10	>64	>64	
12b	OH	*c*Hep	quant	>10	8.6	>64	
9a	-Cl	H	67	>10	>64	>64	
9b	-Cl	*i*Pr	71	>10	>64	>64	
9c	-Cl	*c*Hep	17	2.0	10.0	32	0.32
10a	-Br	H	87	>10	>64	>64	
10b	-Br	*i*Pr	73	>10	>64	>64	
10c	-Br	*c*Hep	88	2.5	34	30	0.32

[a]Isolated yield of the last step. [b]Not tested. [c]Ligand efficiency = $(\Delta G)/N$, where $\Delta G = -RT \ln(IC_{50}(\text{TbrPDEB1}))$ and N is the number of non-hydrogen atoms.[27]

product **9c**. Reductive debenzylation of **8c,d** afforded the phenols **12a,b** required for further derivatization.

A diverse set of benzyl derivatives was introduced on the phenols **12a,b** with either of two MW-assisted nucleophilic substitution protocols to afford inhibitors **13–20a,b** (Scheme 3, Table 2) using substituted bromides or chlorides, where chlorides normally needed longer reaction times for full conversion. For the transformation of nitriles **19a,b** into the corresponding tetrazoles **20a,b** a novel expedient MW-assisted protocol was developed (Scheme 3). Compared to conventional refluxing overnight, the yield was improved from 19% to 62–75% and reaction time was reduced to 1 h.

Pharmacological Measurements. All compounds were tested in at least two independent experiments for inhibition of TbrPDEB1-mediated ^{3}H-cAMP hydrolysis, using scintillation proximity assay and recombinant TbrPDEB1 expressed in Sf21 insect cells, as described previously.[12] The compounds were further tested for inhibition of *T. brucei* bloodstream form trypomastigote proliferation and cytotoxicity on MRC5 fibroblasts using established techniques.[23,24]

To ensure a fast-testing design iteration, assessment of TbrPDEB2 inhibition was omitted at the initial screening stage, as suppression of parasite proliferation would imply concomitant inhibition of TbrPDEB1 and TbrPDEB2. In addition, two previous studies on TbrPDE inhibitors suggest a high degree of equipotency against the paralogues,[12,14] as expected from the high sequence homology. Similarly, the antiparasitic effect of the compounds was constrained to the noninfective disease model subspecies *T. brucei brucei*. The most advanced inhibitor was tested against an extended panel of PDEs, including

dx.doi.org/10.1021/jm301059b | J. Med. Chem. 2012, 55, 8745–8756

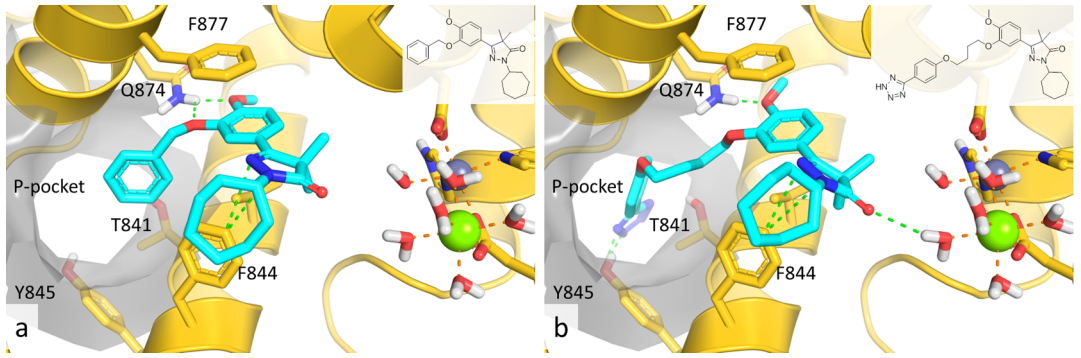

Figure 3. Proposed binding modes of (a) **8d** and (b) **20b** in the TbrPDEB1 homology model. The cycloheptyl rings are folded over the benzene ring of Phe844. The entrance of the P-pocket is occupied by (a) the benzyl moiety of **8d** and (b) the aliphatic tether of **20b** of the tetrazole, which interacts with Tyr845 further into the P-pocket.

Table 2. Inhibitory Potency against TbrPDEB1, *T. b. brucei* Proliferation, and Cytotoxicity of Catechol Pyrazolinones

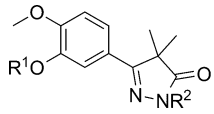

7-12a,b

	R^2 = *i*Pr					R^2 = *c*Hep				
		IC_{50} (μM)		CC_{50} (μM)			IC_{50} (μM)		CC_{50} (μM)	
R^1	compd	TbrPDEB1	*T. b. brucei*	MRC5	LE[a]	compd	TbrPDEB1	*T. b. brucei*	MRC5	LE[a]
4-CN-benzyl	**13a**	2.0	>64	>64	0.27	**13b**	1.0	9.5	>64	0.25
4-MeO-benzyl	**14a**	2.0	32	>64	0.27	**14b**	0.79	10	>64	0.25
4-MeO-phenethyl	**15a**	0.83	32	48.1	0.28	**15b**	0.63	8.1	>64	0.25
1-naphthylmethyl	**16a**	0.79	9.6	>64	0.27	**16b**	0.25	9.6	>64	0.26
2-pyridinmethyl	**17a**	2.5	35	>64	0.28	**17b**	0.50	2.5	>64	0.28
3-(5-methylisoxazolyl)methyl	**18a**	5.0	33	>64	0.27	**18b**	0.63	8.4	33	0.27
4-(4-cyano-phenyloxy)butyl	**19a**	5.0	9.1	>64	0.22	**19b**	0.16	2.3	>64	0.25
4-(4-tetrazolephenyloxy)butyl	**20a**	0.40	2.0	>64	0.24	**20b**	0.049	0.52	>64	0.25

[a]Ligand efficiency = $(\Delta G)/N$, where $\Delta G = -RT \ln(IC_{50}(\text{TbrPDEB1}))$ and N is the number of non-hydrogen atoms.[27]

TbrPDEB2, and trypanosome species. The inhibition of the isolated catalytic domain of TbrPDEB1 was determined using the PDELight HTS cAMP phosphodiesterase kit.[25,26]

Fragment Growing. Compared to hit structure **6a**, the benzyl analogue **8a** was slightly more potent (IC_{50} = 6.3 μM, Table 1), possibly attributed to a $\pi-\pi$ interaction between the phenyl ring of **8a** and Phe844 in the binding pocket. By introduction of aliphatic substituents (R^2) on the nitrogen atom in the pyrazolinone ring, the IC_{50} values could be further improved in a size-dependent manner (R^2 = *c*Hep < *i*Pr < Me ~ H) and submicromolar activities were observed for the cycloheptyl derivatives (e.g., **8d** IC_{50} = 0.50 μM). According to our docking studies, this gain appears to result from the hydrophobic interaction with Phe844 and slightly shifted positioning of the pyrazolinone ring, strengthening the $\pi-\pi$ interactions with Phe844 (Figure 3a). Removal of the catechol ether (**12a,b**) or replacing it with a chloride or bromide (**9**, **10a–c**) was not tolerated, although measurable potencies were observed for the two cycloheptyl derivatives **9**, **10c**. An analysis of the ligand efficiencies (LEs)[27] of this series indicates that with the 24-fold improvement in IC_{50} values the LE values remain constant. Whereas the cyclopentyl derivatives **6a,b** were moderately active in the TbrPDEB1 enzyme assay, no antiproliferative effect was observed in the parasite assay (Table 1). In contrast, the benzyloxy derivatives **8a,c,d** all inhibited parasite proliferation with IC_{50} < 10 μM, without being cytotoxic in MRC5 cells in this concentration range. The difference in antiproliferative efficacy might be attributed to differential parasite cell membrane permeability.

The observed antitrypanosomal efficacy in combination with expedient synthetic access to analogues led us to proceed with the benzyl catechol chemotype. In the docking poses, the benzene ring of these compounds is accommodated at the entrance of the P-pocket, suggesting that it should be possible to grow the inhibitors further into this pocket from the 4-position, which is directed toward the P-pocket channel (Figure 3a). It was, for example, hypothesized that Thr841 in the P-pocket could be targeted by H-bond acceptors. We therefore synthesized the nitriles **13a,b** and anisoles **14a,b**, providing opposite electronic influences on the aromatic ring. In addition, methoxy derivatives with a two-carbon spacer (**15a,b**), as well as naphthyl-substituted analogues **16a,b**, were synthesized to monitor the size of the P-pocket. As the pyrazolinones with R^2 = isopropyl provided better LEs (0.30) and ligand–lipophilicity efficiencies (LLEs, Table 2 in Supporting Information)[28] while good potencies were observed for R^2 = cycloheptyl in the first series, both analogues were synthesized and evaluated. As can be seen in Table 2, all analogues were active TbrPDEB1 inhibitors with IC_{50} values in the range of the parent

dx.doi.org/10.1021/jm301059b | J. Med. Chem. 2012, 55, 8745–8756

compounds **8c,d**. In fact, naphthyl **16b** provided a further 2-fold increase in IC_{50}.

The phenyl of **8c,d** was also replaced with *o*-pyridine (**17a,b**) and 5-methylisoxazol (**18a,b**) rings in order to potentially pick up an additional hydrogen bond with the second hydrogen of the Gln874 nitrogen, uniquely accessed from the P-pocket. However, this approach did not result in an increase in activity (Table 2). Interestingly, as in the previously identified TbrPDEB1 inhibitor **1**, a butyloxy spacer could be incorporated to tether the benzonitriles (**19a,b**) without major loss of activity; in fact, the cycloheptyl derivative **19b** was even more potent than **13b** with an IC_{50} of 0.16 μM (Table 2).

Inspired by the structure of the very potent tetrazole-encompassing tetrahydrophthalazinone **1**,[12] nitriles **19a,b** were converted to the corresponding tetrazoles **20a,b**. This transformation afforded **20b** (VUF13525), which rewardingly proved to be an efficacious inhibitor of TbrPDEB1 (IC_{50} = 49 nM) (Table 2). Docking studies of **20b** indicated that the increase in affinity could be attributed to interactions with residues in the P-pocket (Figure 3b). The proposed conformation of the catechol group is similar to the one of rolipram in its hPDE4 cocrystals[29,30] and shows that the extended alkyl chain is able to reach and enter the P-pocket. This potentially displaces water from the length of the P-pocket and places the tetrazole at the solvent-exposed exit of the pore. In addition, the tetrazole may also form a hydrogen bond with Tyr845, further stabilizing the conformation. Both suggestions may explain the high activity of **20b** and indicate that targeting the P-pocket may be an effective strategy for the design of potent TbrPDEB1 inhibitors.

The antitrypanosomal potency did not strictly follow the same trend as the TbrPDEB1 inhibitory activities in this series of analogues (Table 2 and Chart 1 of Supporting Information). The addition of lipophilic substituents on the benzyl group R^1 often led to low IC_{50} values in the enzymatic assay but not in the parasitic assay (c.f. **13a** and **16b**, Table 2). Moreover, we are also aware of the high cLogP[31] values (Table 1, Supporting Information) of many of the cycloheptyl derivatives, accompanied with reduced aqueous solubility (visual observation), which may have been troubling the whole cell parasite assays to some extent. Yet the most potent TbrPDEB1 inhibitor **20b**, carrying a solubilizing charged tetrazole group, concentration-dependently reduced proliferation of *T. b. brucei* in the cellular assay at submicromolar concentrations (IC_{50} = 520 nM, Table 2). Compound **20b** was therefore analyzed in a broader set of assays (Table 3). As could be expected on the basis of the high homology (88% sequence identity) between the catalytic domains of the TbrPDEB1 and B2 isoenzymes, **20b** also acted as a potent TbrPDEB2 inhibitor (IC_{50} = 72 nM).

Table 3. Pharmacological Profiling of Pyrazolinone 20b

enzymatic assay	IC_{50} (μM)	cellular assay	IC_{50} (μM)
TbrPDEB1	0.049	*T. b. brucei*	0.52
TbrPDEB2	0.072	*T. b. rhodesiense*	0.06
TbrPDEB1 catalytic domain	0.055	*T. cruzi*	7.6
LmjPDEB1	0.13	MRC5	>64[a]
hPDE4A1	0.0021		
hPDE4B1	0.0046		
hPDE4C1	0.010		
hPDE4D3	0.0012		

[a]Mouse macrophage cytotoxicity was observed at 64 μM.

Similarly, the inhibition of the isolated TbrPDEB1 catalytic domain using the PDE light assay[25,26] remained invariant (IC_{50} = 55 nM), suggesting that **20b** is not binding to any allosteric sites such as the GAF domains. To evaluate the selectivity across the PDE families, **20b** was also tested against a panel of other PDE enzymes (Table 3). The *L. major* orthologue LmjPDEB1 was inhibited with a slightly lower potency (IC_{50} = 0.13 μM). On the other hand **20b** was more potent to inhibit representative isoenzymes of PDE4A–D families (IC_{50} at 0.0012–0.010 μM). The relatively low bias for hPDE4 inhibition (4- to 35-fold), compared to piclamilast **2** (>1000-fold), might be attributed to the proposed interactions with the parasite-specific P-pocket. Nevertheless, the data indicate that the binding mode of the compounds in TbrPDEB1 and hPDE4 still needs careful consideration. Evidently, the flexibility of the ligands and/or the hPDE4 protein allows accommodation in the binding site. Considering that the clinical development of hPDE4 inhibitors has been accompanied by emesis and adverse gastrointestinal and proinflammatory side effects,[32,33] the level of hPDE4 inhibition must be considered. The selectivity ratio needed for a safe PDE-targeting trypanocidal is difficult to predict at this stage. The narrow therapeutic window of hPDE4 inhibitors that have advanced to clinical trials indicates that at least equipotency is preferred and most likely future lead optimization efforts should focus on a 10- to 100-fold selectivity for the parasite PDE.

Interestingly, besides being a good inhibitor of *T. b. brucei* proliferation, **20b** was also an excellent inhibitor of *T. b. rhodesiense* (IC_{50} = 60 nM, Table 3), the causative agent of acute East-African HAT, for which the only treatment is the arsenic-containing drug melarsoprol, associated with fatal encephalopathy in 5–10% patients.[34] Moreover, **20b** also showed some activity against *T. cruzi*, the causative agent of Chagas disease.[35] Pyrazolinone **20b** was well-tolerated by the human fibroblast cell line (CC_{50} > 64 μM) and murine macrophages, providing a sensitivity index of at least 250-fold for *T. b. rhodesiense*, i.e., well within the conventional thresholds.[36]

To confirm that the trypanocidal effect of **20b** acts via PDE inhibition, the accumulation of intracellular trypanosomal cAMP was monitored using a FRET-based cAMP sensor that was recombinantly expressed in procyclic trypanosomes. As can be seen in Figure 4a, administration of **20b** to the parasites induced a rapid and dose-dependent increase in intracellular cAMP levels, implying fast penetration over the cellular membrane. When wild-type blood-form *T. b. brucei* was incubated with **20b** for 12 h, it displays the typical phenotype associated with duplicate or multiple nuclei and kinetoplasts (Figure 4b–d), which has previously been observed in genetic[11] and chemical[12] interference of TbrPDE function. The occurrence of aberrant forms of parasites increased with the doses of **20b** administrated. After 48 h of incubation with 10 μM **20b**, parasite cells had lysed confirming the cidal effect of prolonged exposure of TbrPDEB family inhibitors.

CONCLUSIONS

With this study it has been shown that P-pocket directed design of TbrPDEB1 inhibitors is a successful strategy to find highly potent antitrypanosomal compounds. Structure-based and ligand-efficiency-led design resulted in the cathecol pyrazolinone (**20b**) with nanomolar potencies against both TbrPDEB1 and TBrPDEB2 (49 and 72 nM, respectively). It also shows excellent in vitro activity against *T. b. brucei* and, clinically more

dx.doi.org/10.1021/jm301059b | J. Med. Chem. 2012, 55, 8745–8756

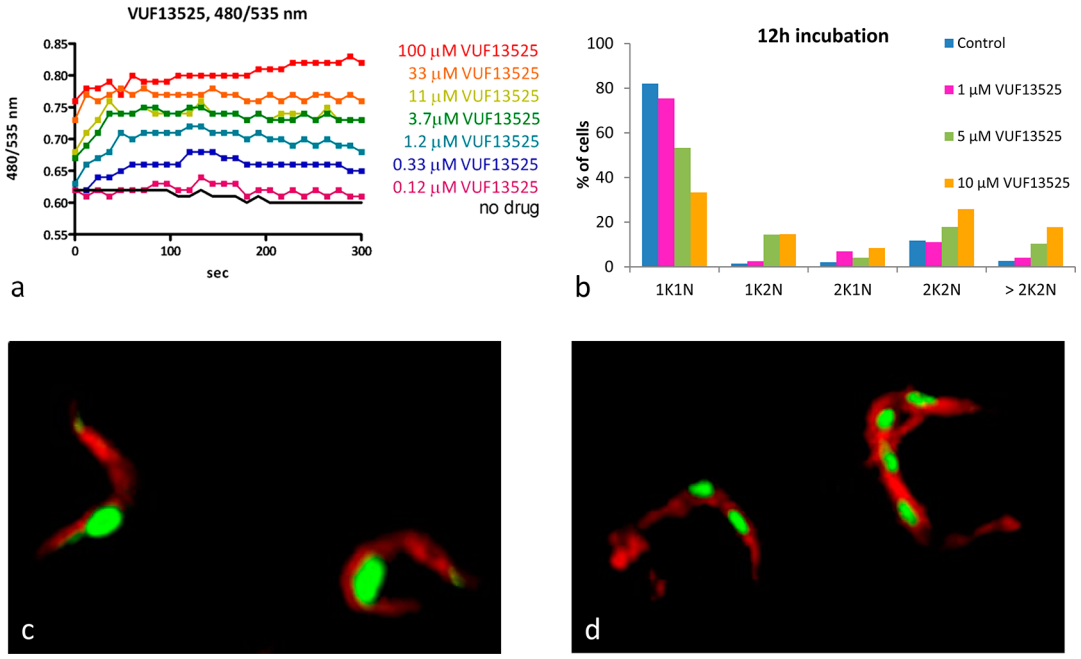

Figure 4. (a) Time−response curves after administration of TbrPDEB1 inhibitor **20b** to engineered *T. brucei* expressing cAMP-FRET sensors. (b) Occurrence of different *T. b. brucei* phenotypes after 12 h of incubation with **20b**: 1N1K (1 nucleus + 1 kinetoplast); 1N2K (1 nucleus + 2 kinetoplasts); 2N1K (2 nuclei + 1 kinetoplast); >2N2K (aberrant forms with more than 2 nuclei and/or 2 kinetoplasts). Microscope images of (c) control *T. b. brucei* 1N1K parasites and (d) *T. b. brucei* parasites after 12 h of incubation with 10 μM pyrazolinone **20b** displaying (left) duplicate nuclei and (right) multiple nuclei and kinetoplasts.

relevant, *T. b. rhodesiense* (60 nM), which is the causative agent of the acute East-African form of HAT. At prolonged exposure, the inhibitor also has a cidal effect on the parasites. On the contrary, mammalian cell lines seem to tolerate the catechol pyrazolinone chemotype very well; fibroblast toxicity was only observed for a handful of compounds.

For the first time, the increase in cAMP levels in the parasites upon administration of PDE inhibitors could be followed in real-time using a FRET-based cAMP sensor expressed in engineered trypanosomes. Being aware of the many challenges that remain, such as selectivity over hPDE4, blood−brain barrier penetration, acceptable pharmacokinetic profile, and metabolic stability, we still believe that the promising pharmacological profile of **20b** brings new hope to the prospect of developing a less toxic alternative to melarsoprol.

EXPERIMENTAL SECTION

Homology Model of TbrPDEB1. The homology model was constructed using the TbrPDEB1 sequence published by Zoraghi and Seebeck (Uniprot code Q8WQX9).[9] The closest homologue of TbrPDEB1 crystallized to date is *Leishmania major* PDEB1, and the structure is published as 2R8Q on the RCSB Protein Data Bank. Aligning the sequences using ClustalW, version 2.1,[37] gave a sequence identity of 66%. The residues on the surface of the catalytic site show an even higher homology with only one substitution (V836I). The P-pocket region has two substitutions, N881M and R885K, both on the far side of the P-pocket from the invariant glutamine (G874).

The homology model was built using the Molecular Operating Environment (MOE), version 2010.10, software package.[38] The B chain of the LmjPDEB1 structure was used to construct the homology model, since the B chain showed lower B factors in the region of the catalytic site. The LmjPDEB1 structure was opened in MOE, and all solvent and metal atoms were removed. The TbrPDEB1 sequence was added and the sequence alignment from ClustalW 2.1 applied. Those residues that were identical in both sequences had their atoms tethered at 200 in the 2R8Q.B model. The Amber99 force field and Born solvation model were used during the homology model construction. There were 10 main chain and 1 side chain models formed. The intermediate models were refined to an rms of 0.1, and the final model was refined once more to an rms of 0.5. Models were protonated using the Protonate 3D function prior to refinement and scored using the GB/VI scoring function. The final model had the metal ions and the six metal-coordinating water molecules included directly from the LmjPDEB1 model, with the hydrogen atoms minimized following inclusion.

The full-length amino acid sequences of the TbrPDEB1 and TbrPDEB2 (Uniprot code Q38F42) catalytic domains were aligned using ClustalW, version 2.1, giving a sequence identity of 75%. Restricting the sequence alignment to the 334 residues of the catalytic domain increased the sequence identity to 88%.

Inhibitor Docking. The structures of the ligands were prepared in MOE and exported as an SDF database. A single low energy conformation was generated for each structure using Omega 2.4.3, OpenEye Scientific Software.[39] The mol2 file generated by Omega was used as input for GOLD.[40] The compounds were docked into the homology model of TbrPDEB1 described above, which was used as prepared. GOLD uses a genetic algorithm to efficiently explore the conformational space of the ligand in the protein pocket. The parameters used in GOLD include autoscaling of operations per ligand (dependent on the number of rotatable bonds), PLP scoring function, water included with spin, metal ions included, and the generation of 30 solutions per ligand with an rms tolerance of 1.5 Å. Results were analyzed using MOE, and binding poses were rendered in PyMOL.[41]

Synthetic Chemistry. General Information. Chemicals and reagents were purchased from commercial suppliers and were used without further purification. Microwave reactions were performed with Biotage Initiator single mode cavity, producing controlled irradiation at 2450 MHz in sealed reaction vials (capable of withholding elevated pressure) and with magnetic stirring. For column chromatography commercially available silica gel 60 (particle size 0.040−0.063 mm) was used. Gradient flash column chromatography purification was performed on Biotage Isolera with prepacked silica (KP-sil) cartridges supplied by Biotage and ethyl acetate in *n*-heptane as eluent, unless otherwise stated. Analytical thin layer chromatography was performed

dx.doi.org/10.1021/jm301059b | J. Med. Chem. 2012, 55, 8745−8756

using glass sheets precoated with silica gel 60 F_{254}, and visualization of components was made by UV (254 nm), I_2, and/or Pancaldi's solution followed by heating. Analytical HPLC−MS was performed on a Shimadzu LC-20AD liquid chromatography pump system with a Shimadzu LCMS-2010 liquid chromatography mass spectrometer equipped with Xbridge (C18) 5 μm column (50 mm × 4.6 mm), using acetonitrile in 0.10% aqueous formic acid and a 5−90% gradient over 4.5 min followed by a 2 min isocratic 90% mobile phase. ^{1}H NMR and ^{13}C NMR spectra were measured on a Bruker 200, 400, or 500 instrument at 250, 400, or 500 MHz, respectively. The chemical shifts for ^{1}H NMR and ^{13}C NMR were referenced to TMS via the $CDCl_3$ solvent signal (^{1}H NMR at 7.26 ppm and ^{13}C NMR at 77.16 ppm). Exact molecular masses (HRMS) were determined on a Bruker micrOTOF-Q mass spectrometer equipped with an electrospray ion source using caffeine as reference. The purity for all compounds was established to be ≥95% by HPLC, ^{1}H NMR, and ^{13}C NMR, unless otherwise stated. Acyl chloride precursors of β-keto esters **11a**−**d**[42−45] are known compounds. The synthetic preparation and spectroscopic data of catechol pyrazolinone **8a** have previously been published in a patent.[20]

Experimental Details and Spectroscopic Data for Precursors 11a,b. Methyl 3-(3-(Cyclopentyloxy)-4-methoxyphenyl)-2,2-dimethyl-3-oxopropanoate (11a). 3-(Cyclopentyloxy)-4-methoxybenzoic acid (5.0 g, 21.1 mmol) was suspended in 25 mL of dry DCM, and DMF (3 drops) was added. Oxalyl chloride (2.78 mL, 31.7 mmol) was added dropwise under vigorous stirring and N_2 atmosphere. The reaction mixture was stirred at room temperature for 1.5 h. The reaction was monitored with TLC of small aliquots of the reaction mixture, which were diluted with MeOH and heated with a heat gun. When full conversion was observed, the volatiles were evaporated in vacuo to give 3-(cyclopentyloxy)-4-methoxybenzoyl chloride as a yellow crystalline solid, which was used as such in the subsequent step without any further purification.

Lithium diisopropylamide (13 mL, 1.8 M in THF/hexane/ether, 1.1 equiv) was added to a dry three-neck flask with 25 mL of freshly distilled THF and cooled to −45 °C, and methyl isobutyrate (3.64 mL, 31.7 mmol, 1.5 equiv) was added dropwise. The mixture was stirred for 30 min at −40 °C. Freshly prepared 3-(cyclopentyloxy)-4-methoxybenzoyl chloride (approximately 21 mmol) was dissolved in dry THF (25 mL) and added dropwise during 30 min at −50 to −40 °C. The reaction mixture was stirred for another 1 h before the cooling source was removed, and the stirring continued at room temperature overnight. The reaction mixture was acidified with 3 M HCl (aq) and diluted with EtOAc (10 mL), and the aqueous layer was extracted with EtOAc (2 × 10 mL). The combined organic layers were washed with saturated $NaHCO_3$ and brine, dried over $MgSO_4$, and reduced in vacuo. The crude product was purified with flash chromatography to give the title compound as a pale syrup (1.1 g, 15%): ^{1}H NMR (500 MHz, $CDCl_3$) δ (ppm) 7.50−7.41 (m, 2H), 6.83 (d, J = 9.08 Hz, 1H), 4.82−4.73 (m, 1H), 3.83 (s, 3H), 3.64 (s, 3H), 2.07−1.94 (m, 2H), 1.94−1.75 (m, 4H), 1.72−1.59 (m, 2H), 1.54 (s, 6H); ^{13}C NMR (126 MHz, CDCl3) δ (ppm) 196.14, 176.13, 153.94, 147.59, 127.85, 122.77, 114.49, 110.64, 80.55, 56.18, 53.09, 52.66, 32.93, 24.33, 24.31; LC−MS-ESI$^+$ found 321 $[M + H]^+$.

Methyl 3-(3-(Benzyloxy)-4-methoxyphenyl)-2,2-dimethyl-3-oxopropanoate (11b). Following the procedure to **11b** using 3-(benzyloxy)-4-methoxybenzoic acid on a 148 mmol scale first gave 3-(benzyloxy)-4-methoxybenzoyl chloride as a yellow semisolid (41.5 g, quantitative, >95% purity according to ^{1}H NMR): ^{1}H NMR (250 MHz, $CDCl_3$) δ (ppm) 7.78 (dd, J = 8.45, 1.94 Hz, 1H), 7.66 (d, J = 1.90 Hz, 1H), 7.48 (d, J = 7.26 Hz, 2H), 7.43−7.28 (m, 3H), 6.94 (d, J = 8.52 Hz, 1H), 5.30 (s, 1H), 5.19 (s, 3H), 3.95 (s, 3H). The title compound was produced as a yellow syrup (59 g, quantitative, 90% purity): ^{1}H NMR (250 MHz, $CDCl_3$) δ (ppm) 7.55−7.44 (m, 4H), 7.43−7.26 (m, 3H), 6.88 (d, J = 8.4 Hz, 1H), 5.18 (s, 2H), 3.94 (s, 3H), 3.61 (s, 3H), 1.51 (s, 6H); ^{13}C NMR (63 MHz, $CDCl_3$) δ (ppm) 195.81, 175.85, 153.58, 147.94, 136.54, 128.63, 128.05, 127.85, 127.49, 123.30, 113.78, 110.59, 70.85, 56.06, 52.97, 52.47, 24.13; LC−MS-ESI$^+$ found 343 $[M + H]^+$.

Experimental Details and Spectroscopic Data for Pyrazolinones. 3-(3-(Cyclopentyloxy)-4-methoxyphenyl)-4,4-dimethyl-1*H*-pyrazol-5(4*H*)-one (6a). To a reaction tube with **11a** (0.851 g, 2.66 mmol) dissolved in ethanol (5.5 mL, 0.5 M reaction molarity) was added aqueous hydrazine hydrate (80%, 1.4 mL, 8 equiv). The reaction mixture was stirred at 50 °C overnight. The reaction mixture was cooled on ice and the precipitate was filtered off over a glass filter, washed with cold ethanol, and dried at 40 °C under vacuum to give the title compound as a solid foam (0.72 g, 90%): ^{1}H NMR (400 MHz, $CDCl_3$) δ (ppm) 9.43 (s, 1H), 7.42 (d, J = 1.93 Hz, 1H), 7.27 (dd, J = 8.35, 2.06 Hz, 1H), 6.86 (d, J = 8.46 Hz, 1H), 4.92−4.69 (m, 1H), 3.87 (s, 3H), 2.04−1.74 (m, 6H), 1.71−1.55 (m, 2H), 1.51 (s, 6H); ^{13}C NMR (101 MHz, $CDCl_3$) δ (ppm) 181.71, 163.35, 151.93, 148.11, 123.93, 119.36, 112.34, 111.41, 80.68, 56.13, 47.40, 32.93, 24.21, 22.85; LC−MS-ESI$^+$ found 303 $[M + H]^+$; HRMS-ESI$^+$ $[M + H]^+$ calcd for $C_{17}H_{23}N_2O_3$ 303.1703, found 303.1698.

1-Cycloheptyl-3-(3-(cyclopentyloxy)-4-methoxyphenyl)-4,4-dimethyl-1*H*-pyrazol-5(4*H*)-one (6b). Sodium hydride (52 mg, 1.3 mmol, 2 equiv) was added to a chilled suspension of **6a** (195 mg, 0.65 mmol) in DMF/MeCN (2:1) under stirring and N_2 atmosphere. The reaction mixture was stirred for 15 min before bromocycloheptane (0.31 mL, 2.3 mmol, 3.5 equiv) was added. The reaction mixture was heated at 120 °C overnight. The volatiles were evaporated in vacuo. The residue was diluted with EtOAc (50 mL) and washed with brine (3 × 15 mL), dried over Na_2SO_4, filtered, and reduced in vacuo. The residue was purified via flash chromatography to give the title compound as a pale solid (230 mg, 89% yield): ^{1}H NMR (400 MHz, $CDCl_3$) δ (ppm) 7.39 (d, J = 1.90 Hz, 1H), 7.28 (dd, J = 8.47, 1.90 Hz, 1H), 6.85 (d, J = 8.47 Hz, 1H), 4.91−4.72 (m, 1H), 4.37−4.18 (m, 1H), 3.86 (s, 3H), 2.03−1.72 (m, 12H), 1.72−1.47 (m, 8H), 1.43 (s, 6H); ^{13}C NMR (126 MHz, $CDCl_3$) δ (ppm) 177.50, 161.48, 151.59, 147.82, 124.10, 119.35, 112.55, 111.35, 80.69, 56.07, 54.57, 48.58, 33.43, 32.95, 28.33, 24.81, 24.27, 22.86; LC−MS-ESI$^+$ m/z 399 $[M + H]^+$; HRMS-ESI$^+$ $[M + H]^+$ calcd for $C_{24}H_{35}N_2O_3$ 399.2642, found 399.2624.

3-(3-(Benzyloxy)-4-methoxyphenyl)-4,4-dimethyl-1*H*-pyrazol-5(4*H*)-one (8a). Following the procedure to **6a** using **11b** on a 0.15 mol scale gave the title compound as a yellow solid (47.36 g, 97%): ^{1}H NMR (400 MHz, $CDCl_3$) δ (ppm) 9.67 (br s, 1H), 7.44 (appar d, J = 7.36 Hz, 2H), 7.41 (d, J = 1.93 Hz, 1H), 7.39−7.26 (m, 4H), 6.89 (d, J = 8.48 Hz, 1H), 5.18 (s, 2H), 3.91 (s, 3H), 1.41 (s, 6H); ^{13}C NMR (101 MHz, $CDCl_3$) δ (ppm) 181.72, 163.11, 151.49, 148.35, 136.85, 128.68, 128.05, 127.39, 123.88, 119.99, 111.78, 111.38, 71.16, 56.07, 47.32, 22.62; LC−MS-ESI$^+$ m/z 325 $[M + H]^+$; HRMS-ESI$^+$ $[M + H]^+$ calcd for $C_{19}H_{21}N_2O_3$ 325.1547, found 325.1531.

3-(3-(Benzyloxy)-4-methoxyphenyl)-1-isopropyl-4,4-dimethyl-1*H*-pyrazol-5(4*H*)-one (8c). Following the procedure to **6b** using isopropyl bromide and **8a** on a 2.46 mmol scale gave the title compound as a white solid (706 mg, 78%): ^{1}H NMR (400 MHz, $CDCl_3$) δ (ppm) 7.49 (d, J = 7.3 Hz, 2H), 7.44 (d, J = 1.9 Hz, 1H), 7.34 (m, 4H), 6.91 (d, J = 8.5 Hz, 1H), 5.22 (s, 2H), 4.50 (hept, J = 6.7 Hz, 1H), 3.93 (s, 3H), 1.38 (s, 6H), 1.37 (d, J = 7.0 Hz, 6H); ^{13}C NMR (101 MHz, $CDCl_3$) δ (ppm) 177.85, 161.28, 151.30, 148.28, 137.00, 128.66, 128.05, 127.47, 124.11, 119.92, 112.17, 111.38, 71.36, 56.06, 48.73, 45.26, 22.67, 20.82; LC−MS-ESI$^+$ m/z 367 $[M + H]^+$; HRMS-ESI$^+$ $[M + H]^+$ calcd for $C_{22}H_{27}N_2O_3$ 367.2016, found 367.1998.

3-(3-(Benzyloxy)-4-methoxyphenyl)-1-cycloheptyl-4,4-dimethyl-1*H*-pyrazol-5(4*H*)-one (8d). Following the procedure to **6b** on a 1.59 mmol scale using **8a** gave the title compound as a white solid (544 mg, 81% yield): ^{1}H NMR (400 MHz, $CDCl_3$) δ (ppm) 7.49−7.43 (m, 2H), 7.41 (d, J = 2.00 Hz, 1H), 7.38−7.33 (m, 2H), 7.32−7.26 (m, 2H), 6.87 (d, J = 8.49 Hz, 1H), 5.20 (s, 2H), 4.36−4.16 (m, 1H), 3.90 (s, 3H), 1.98−1.74 (m, 6H), 1.67−1.47 (m, 6H), 1.34 (s, 6H); ^{13}C NMR (101 MHz, $CDCl_3$) δ (ppm) 177.41, 161.16, 151.21, 148.23, 136.98, 128.61, 127.99, 127.38, 124.09, 119.83, 112.10, 111.32, 71.31, 56.02, 54.47, 48.39, 33.39, 28.34, 24.73, 22.62; LC−MS-ESI$^+$ m/z 421 $[M + H]^+$; HRMS-ESI$^+$ $[M + H]^+$ calcd for $C_{26}H_{33}N_2O_3$ 421.2486, found 421.2467.

3-(3-Hydroxy-4-methoxyphenyl)-1-isopropyl-4,4-dimethyl-1*H*-pyrazol-5(4*H*)-one (12a). Ammonium formate (10 g, 159 mmol) and 10% Pd/C (50 mg, 0.047 mmol) were added to benzyl ether **8c** (12 g, 32.7 mmol) dissolved in MeOH/CH_2Cl_2 (2:1, 200 mL). The reaction mixture was stirred for 5 h at 40 °C. The reaction mixture was filtered through a cake of Celite, and the volatiles were evaporated. The residue was diluted with EtOAc, washed with brine (2 × 200 mL), dried over Na_2SO_4, filtered, and reduced in vacuo with CH_2Cl_2 as cosolvent to give the title compound as an off-white solid (8.73 g, 96% yield): ^{1}H NMR (400 MHz, $CDCl_3$) δ 7.44 (d, J = 2.0 Hz, 1H), 7.29 (dd, J = 8.4, 2.0 Hz, 1H), 6.86 (d, J = 8.5 Hz, 1H), 5.97 (s, 1H), 4.49 (hept, J = 6.6 Hz, 1H), 3.92 (s, 3H), 1.44 (s, 6H), 1.34 (d, J = 6.7 Hz, 6H); ^{13}C NMR (101 MHz, $CDCl_3$) δ (ppm) 178.06, 161.60, 148.22, 145.99, 124.91, 118.78, 112.61, 110.62, 56.10, 49.00, 45.37, 22.74, 20.85; LC−MS-ESI$^+$ m/z 277 $[M + H]^+$; HRMS-ESI$^+$ $[M + H]^+$ calcd for $C_{15}H_{21}N_2O_3$ 277.1547, found 277.1543.

1-Cycloheptyl-3-(3-hydroxy-4-methoxyphenyl)-4,4-dimethyl-1*H*-pyrazol-5(4*H*)-one (12b). Following the procedure of **12a** using **8d** on a 1.32 mmol scale afforded the title compound as a pale oil (1.35 g, quantitative yield, 99.8% purity): ^{1}H NMR (400 MHz, $CDCl_3$) δ (ppm) 7.46 (d, J = 2.05 Hz, 1H), 7.29 (dd, J = 8.43, 2.08 Hz, 1H), 6.87 (d, J = 8.49 Hz, 1H), 6.30 (br s, 1H), 4.36−4.22 (m, 1H), 3.92 (s, 3H), 2.03−1.74 (m, 6H), 1.70−1.47 (m, 6H), 1.45 (s, 6H); ^{13}C NMR (101 MHz, $CDCl_3$) δ 177.62, 161.58, 148.30, 146.00, 124.72, 118.64, 112.63, 110.63, 56.00, 54.58, 48.66, 33.37, 28.25, 24.72, 22.61; LC−MS-ESI$^+$ m/z 331 $[M + H]^+$; HRMS-ESI$^+$ $[M + H]^+$ calcd for $C_{19}H_{27}N_2O_3$ 331.2016, found 331.1997.

General Procedure to O-Alkylations A. Corresponding phenol **12a** or **12b** was added to a MW reaction tube with K_2CO_3 (3.0 equiv) and MeCN/DMF (1:1, 0.2 M final reaction molarity). It was MW irradiated for 30 min at 120 °C. After releasing the CO_2 gas from the MW tube, the corresponding bromide or chloride (2 equiv) was added via a needle through the septum. The reaction mixture was again MW irradiated for 20 min at 120 °C. In the case of low conversion, an addition 1 equiv of halide was added and the reaction mixture was reirradiated for 40 min. The volatiles were evaporated in vacuo. The residue was dissolved in EtOAc and the organic layer was washed with brine and brine with saturated NH_4Cl, 1:1. The organic phase was dried over Na_2SO_4, filtered, and reduced in vacuo. The crude product was purified using gradient flash column chromatography.

General Procedure to O-Alkylations B. Sodium hydride (60% dispersed in oil, 2−5 equiv) was added to corresponding phenol **12a** or **12b** dissolved in DMF (0.14 M reaction molarity) under N_2 atmosphere. The mixture was stirred for 5−15 min prior to addition of the corresponding bromide (1.5 equiv). The reaction mixture was microwave irradiated at 120 °C for 15−30 min and then worked up as in general procedure A.

4-(4-(5-(1-Isopropyl-4,4-dimethyl-5-oxo-4,5-dihydro-1*H*-pyrazol-3-yl)-2-methoxyphenoxy)butoxy)benzonitrile (19a). Following the general procedure A on a 1.12 mmol scale gave the title compound as an off-white solid (201 mg, 40%): ^{1}H NMR (400 MHz, $CDCl_3$) δ (ppm) 7.59−7.50 (m, 2H), 7.45 (d, J = 1.96 Hz, 1H), 7.29−7.23 (m, 1H), 6.96−6.88 (m, 2H), 6.85 (d, J = 8.46 Hz, 1H), 4.48 (hept, J = 6.70 Hz, 1H), 4.13 (dt, J = 14.51, 5.74 Hz, 4H), 3.85 (s, 3H), 2.08−2.00 (m, 4H), 1.44 (s, 6H), 1.35 (d, J = 6.72 Hz, 6H); ^{13}C NMR (101 MHz, $CDCl_3$) δ 177.95, 162.44, 161.51, 151.17, 148.76, 134.08, 124.27, 119.78, 119.39, 115.33, 111.13, 110.63, 103.90, 68.71, 68.13, 56.07, 48.94, 45.40, 26.14, 25.91, 22.97, 20.93; LC−MS-ESI$^+$ m/z 450 $[M + H]^+$; HRMS-ESI$^+$ $[M + H]^+$ calcd for $C_{26}H_{32}N_3O_4$ 450.2387, found 450.2366.

4-(4-(5-(1-Cycloheptyl-4,4-dimethyl-5-oxo-4,5-dihydro-1*H*-pyrazol-3-yl)-2-methoxyphenoxy)butoxy)benzonitrile (19b). Following the general procedure B on a 0.58 mmol scale gave the title compound as an off-white solid (166 mg, 57%): ^{1}H NMR (400 MHz, $CDCl_3$) δ (ppm) 8.11 (appar d, J = 8.85 Hz, 2H), 7.42 (d, J = 1.98 Hz, 1H), 7.32 (dd, J = 8.43, 1.99 Hz, 1H), 7.01 (appar d, J = 8.88 Hz, 2H), 6.88 (d, J = 8.53 Hz, 1H), 4.35−4.26 (m, 1H), 4.18 (t, J = 5.97 Hz, 2H), 4.13 (t, J = 5.75 Hz, 2H), 3.89 (s, 3H), 2.11−1.94 (m, 6H), 1.94−1.84 (m, 2H), 1.84−1.73 (m, 2H), 1.69−1.50 (m, 6H), 1.49 (s, 6H); ^{13}C NMR (101 MHz, $CDCl_3$) δ (ppm) 178.14, 175.72, 162.46, 161.57, 151.31, 148.69, 129.25, 123.92, 119.98, 116.45, 115.28, 111.31, 110.81, 68.88, 68.02, 56.12, 55.25, 49.24, 33.44, 28.21, 26.19, 26.14, 24.89, 22.88; LC−MS-ESI$^+$ m/z 504 $[M + H]^+$; HRMS-ESI$^+$ $[M + H]^+$ calcd for $C_{30}H_{38}N_3O_4$ 504.2857, found 504.2840.

3-(3-(4-(4-(2*H*-Tetrazole-5-yl)phenoxy)butoxy)-4-methoxyphenyl)-1-isopropyl-4,4-dimethyl-1*H*-pyrazol-5(4*H*)-one (20a). A mixture of compound **19a** (141 mg, 0.31 mmol), sodium azide (203 mg, 3.1 mmol), and NH_4Cl (167 mg, 3.1 mmol) in DMF (6 mL) was MW irradiated at 160 °C for 1 h. The reaction mixture was cooled to room temperature, diluted with EtOAc, and washed twice with brine acidified with HCl (aq). The first aqueous layer was extracted with EtOAc (2 × 5 mL). The combined organic layers were further washed with brine acidified with HCl (aq), reduced, and the crude product was purified with flash column chromatography (eluent MeOH in CH_2Cl_2 with 0.5% AcOH) to afford the title compound as an off-white solid (115 mg, 75%): ^{1}H NMR (500 MHz, $CDCl_3$) δ (ppm) 8.11 (appar d, J = 8.76 Hz, 2H), 7.44 (d, J = 1.71 Hz, 1H), 7.33 (dd, J = 8.42, 1.78 Hz, 1H), 7.02 (appar d, J = 8.79 Hz, 2H), 6.89 (d, J = 8.49 Hz, 1H), 4.54 (hept, J = 6.70 Hz, 1H), 4.19 (t, J = 6.06 Hz, 2H), 4.14 (t, J = 5.77 Hz, 2H), 3.89 (s, 3H), 2.07 (dt, J = 12.48, 6.49 Hz, 4H), 1.49 (d, J = 9.55 Hz, 6H), 1.39 (d, J = 6.70 Hz, 6H); MS-ESI$^+$ (m/z 493, M + H$^+$); ^{13}C NMR (126 MHz, $CDCl_3$) δ (ppm)178.53, 162.43, 161.56, 156.09, 151.29, 148.70, 129.25, 123.82, 119.92, 116.34, 115.26, 111.14, 110.61, 68.82, 67.94, 56.08, 49.50, 45.83, 26.17, 26.06, 22.90, 20.87; LC−MS-ESI$^+$ m/z 493 $[M + H]^+$; HRMS-ESI$^+$ $[M + H]^+$ calcd for $C_{26}H_{33}N_6O_4$ 493.2558, found 493.2545.

3-(3-(4-(4-(2*H*-Tetrazole-5-yl)phenoxy)butoxy)-4-methoxyphenyl)-1-cycloheptyl-4,4-dimethyl-1*H*-pyrazol-5(4*H*)-one (20b). Following the procedure to compound **20a** using nitrile **19b** (100 mg, 0.20 mmol) afforded the title compound as an off-white solid (95 mg, 62%): ^{1}H NMR (500 MHz, $CDCl_3$) δ (ppm) ^{1}H NMR (500 MHz, $CDCl_3$) δ (ppm) 8.14 (d, J = 8.87 Hz, 2H), 7.44 (d, J = 2.05 Hz, 1H), 7.30 (dd, J = 8.46, 2.04 Hz, 1H), 7.01 (d, J = 8.92 Hz, 2H), 6.88 (d, J = 8.53 Hz, 1H), 4.36−4.25 (m, 1H), 4.18 (t, J = 6.00 Hz, 2H), 4.13 (t, J = 5.94 Hz, 2H), 3.88 (s, 3H), 2.12−1.93 (m, 6H), 1.93−1.85 (m, 2H), 1.82−1.73 (m, 2H), 1.67−1.49 (m, 6H), 1.49 (s, 6H); ^{13}C NMR (126 MHz, $CDCl_3$) δ (ppm) 178.14, 162.48, 161.56, 156.14, 151.29, 148.68, 129.27, 123.82, 119.93, 116.36, 115.25, 111.17, 110.66, 68.83, 67.94, 56.09, 55.26, 49.25, 33.41, 28.16, 26.18, 26.05, 24.85, 22.87; LC−MS-ESI$^+$ m/z 547 $[M + H]^+$; HRMS-ESI$^+$ $[M + H]^+$ calcd for $C_{30}H_{39}N_6O_4$ 547.3027, found 547.3015.

Pharmacological Evaluation. Expression of Recombinant TbrPDEB1 and TbrPDEB2. Full length hPDE4A1, B1, C1, and D3 and TbrPDEB1 were expressed in Sf21 insect cells and full length TbrPDEB2 was expressed in yeast, as previously described.[12]

His-tagged catalytic domains of TbrPDEB1 were expressed in *E. coli* BL21 codon plus cells and column purified as recommended in the manual "The Qiaexpressionist" (Qiagen). PDEs were dissolved in 10 mM HEPES buffer (pH 7.4) containing 100 mM NaCl and 5 mM $MgCl_2$.

Determination of PDE Activity. PDE activities were determined according to two different methods throughout the study.

Full Length PDEs. The standard scintillation proximity assay (SPA) for determination of PDE activities was used exactly following the procedure as recently outlined by De Koning et al.[1214] to analyze effects of test compounds on the enzymatic activities of TbrPDEB1, TbrPDEB2, LmjPDEB1, human PDE4A1, 4B1, 4C1, and 4D3. In these assays, the cAMP substrate concentration was 0.5 μM. Briefly, PDE activity of supernatants of sonicated PDE-overexpressing Sf21 cells was determined at least in duplicate by published procedures.[12,46,47] Enzyme concentrations were always adjusted so that <20% of substrate was consumed. Blank values (measured in the presence of denatured protein) were always <2% of total radioactivity.

Catalytic Domain TbrDEB1. The determination of TbrPDEB1 catalytic domain activity was performed with PDELight HTS cAMP phosphodiesterase kit[25,26] in a reaction volume of 50 μL comprising 1% DMSO in a 96 well-format. PDELight assay is a nonradioactive, bioluminescent detection system for measuring the activity of PDEs developed by Lonza Rockland, Inc. This assay was used in the determination of IC_{50} values for inhibitors against catalytic domain of

TbrPDEB1. This assay offers a continuous readout of luminescence based on the following reactions: PDEs hydrolyze cAMP to AMP; AMP is then converted directly to ATP by "AMP-DR", Lonza's proprietary AMP detection reagent; luciferase is then utilized to catalyze the formation of light from luceferin and the newly formed ATP. Luciferase catalysis step also regenerates AMP, and therefore, the light output is linear with the rate of AMP production by the PDE. The reaction uses cAMP at 0.5 μM. From the rate of increase in light intensity over a period of time, the reaction rate is calculated. The reaction output light was monitored at 25 °C for 20 min using Victor2, yielding a specific activity of about 2500 U/min in the given conditions. Dose−response curves were generated by plotting the percent of inhibition of PDE against the inhibitor concentrations. Nonlinear regression analysis was used to calculate IC_{50} values from each dose−response curve by using GraphPad Prism (version 5.01).

In Vitro Susceptibility Testing of Trypanosomes and MRC5 Fibroblasts. *T. b. brucei* (Squib-427 strain, suramin-sensitive) or *T. b. rhodesiense* (STIB-900 strain) trypomastigotes were cultured at 37 °C and 5% CO_2 in Hirumi-9 medium[48] supplemented with 10% fetal calf serum (FCS). Compound stock solutions were prepared in 100% DMSO at 20 mM or mg/mL. The compounds were serially prediluted (2-fold or 4-fold) in DMSO followed by a further (intermediate) dilution in demineralized water to ensure a final in-test DMSO concentration of <1%.

Assays were performed by adding 1.5×10^4 trypomastigotes/well containing the prediluted compounds. After 72 h of incubation, parasite growth was assessed fluorimetrically by adding resazurin[24] for 24 h at 37 °C. Fluorescence was measured using a GENios Tecan fluorimeter (excitation 530 nm, emission 590 nm).

For cytotoxicity evaluation, human fetal lung fibroblasts were cultivated in MEM, supplemented with L-glutamine (20 mM), 16.5 mM sodium hydrogen carbonate, and 5% FCS at 37 °C and 5% CO_2. For the assay, 10^4 MRC-5 cells/well were seeded onto the test plates containing the prediluted compounds and incubated at 37 °C and 5% CO_2 for 72 h. Cell viability was determined after addition of resazurin. Fluorescence was measured using a GENios Tecan fluorimeter (excitation 530 nm, emission 590 nm).[23,49]

Phenotype Determination. *T. b. brucei* trypomastigotes (1×10^6 parasites/mL) were incubated with **20b** (1, 5, or 10 μM or vehicle) for 12 h. Thereafter, parasites were harvested and washed once with saline. Culture aliquots were spread onto glass slides. After drying, they were fixed for 15 min with 2% formaldehyde and stained for 30 min at room temperature with Syto-9 (Invitrogen), 250 nM, and Nyle Red (Sigma), 50 mg/mL. Slides were analyzed using an Olympus BX41 microscope. For each sample, >300 cells were analyzed. Cells were manually scored and assigned to the following categories: 1N1K (1 nucleus + 1 kinetoplast); 1N2K (1 nucleus + 2 kinetoplasts); 2N1K (2 nuclei + 1 kinetoplast); >2N2K (aberrant forms with more than 2 nuclei and/or 2 kinetoplasts).

FRET cAMP Sensor Construct. Expression of cAMP Sensors in Trypanosomes. Nikolaev et al.[50,51] had developed a series of FRET-based cAMP sensors to analyze the spatial and temporal regulation of cAMP signaling in living cells. They are based on a YFP and a CFP fluorescent protein linked to various cAMP-binding domains. For use in trypanosomes, a sensor variant utilizing the cAMP binding domain of EPAC 1[52] ($K_{D(cAMP)} \approx 1$ μM cAMP) was selected. For expression in procyclic trypanosomes, the EPAC 1 sensor was amplified from the corresponding pcDNA3 vector (generously provided by V. Nikolaev) using the following primers: cAMPsensor-fo (5′-TACTCGAGCTATAGGGAGACCC-AAGCTT-3′, underlined XhoI restriction site) and cAMPsensor-re (5′-TAGGATCCTA-GGTGACACTATAGATAG-3′, underlined BamHI restriction site). The PCR product was cloned into the pGAPRONEΔLII-mcs vector (pGΔLII-mcs).[53] The final construct was linearized with SpeI and transfected into the procyclic *T. brucei* strain 427[54] for stable integration into the EP procyclin locus. Transfectants were selected by adding neomycin (1 μg/mL) into the medium. Expression of the EPAC 1 sensor was verified by FACS analysis and by immunofluorescence.

FRET Analysis. Procyclic trypanosomes were cultured in SDM79 medium containing 5% fetal calf serum.[55] For FRET analysis, cells were collected by centrifugation from logarithmically growing culture (50 mL), suspended in 15 mL of Hank's balanced salt solution (HBSS, GIBCO), centrifuged for 10 min at 4000 rpm, and suspended to a final cell density of $(5-6) \times 10^7$/mL in fresh HBSS buffer. Drugs were dissolved in dimethylsulfoxide (DMSO), and appropriate dilution series in DMSO were prepared. Drugs were spotted (1 μL per well) into black, flat-bottom 96-well plates, followed by the addition of 100 μL/well of HBSS and extensive mixing. Plates were allowed to equilibrate at 27 °C in the thermostated chamber of a Gemini Spectramax fluorescence reader. Immediately before FRET recording was started, 100 μL of cell suspension was added to each well and plates were vibrated for 5 s. Fluorescence was then measured using an excitation wavelength of 436 nm while recording the appropriate emissions at 480 and 535 nm, with cutoff filters set at 475 and 530 nm, respectively. After finishing each series, cell motility was checked microscopically. As a positive control, a dilution series of the PDE inhibitor PPS50419[12] was included in each experiment.

■ ASSOCIATED CONTENT

Supporting Information

Synthetic procedures and spectroscopic data of compounds **8b**, **11c,d**, **9**, **10a−c**, **11c,d**, and **13−18a,b**; ^{1}H NMR and ^{13}C NMR spectra of compound **20b**, a graph of the correlation between *T. b. brucei* proliferation inhibition and TbrPDEB1 inhibition of catechol pyrazolinones; and tabulated cLogP values and LLEs for all compounds. This material is available free of charge via the Internet at http://pubs.acs.org.

■ AUTHOR INFORMATION

Corresponding Author

*Phone: +31-20598-7579/7600. E-mail: R.Leurs@vu.nl.

Present Address

●Swiss Transfusion SRC Inc., Laupenstrasse 37, 3001 Bern, Switzerland.

Notes

The authors declare no competing financial interest.

■ ACKNOWLEDGMENTS

This research was performed under the framework of the Top Institute Pharma project "Phosphodiesterase Inhibitors for Neglected Tropical Diseases" with partners VU University Amsterdam, University of Bern, The Royal Tropical Institute, The Netherlands, Mercachem BV, Nycomed (a Takeda company), IOTA Pharmaceuticals Ltd., Drugs for Neglected Diseases *initiative* (DND*i*), and TI Pharma. Shaïsta Bakhtali, Hans Custers, and An Matheeussen are acknowledged for excellent technical assistance and Hermann Tenor for invaluable input to the manuscript and the project in general. DND*i* is grateful to its donors, public and private, who have provided funding to DND*i* since its inception in 2003. With the support of these donors, DND*i* is well on its way to achieving the objectives of building a robust pipeline and delivering 11−13 new treatments by 2018. A full list of DND*i*'s donors can be found at http://www.dndi.org/index.php/donors.html?ids=8. For the work described in this paper, DND*i* allocated non-earmarked funding (Department for International Development (DFID)/United Kingdom, Dutch Ministry of Foreign Affairs (DGIS)/The Netherlands, Federal Ministry of Education and Research (BMBF)/Germany, Spanish Agency for International Development Cooperation (AECID)/Spain, Swiss Agency for Development and Cooperation (SDC)/Switzerland, Médecins Sans Frontières (Doctors without

Borders)/international. The donors had no role in study design, data collection and analysis, decision to publish, or preparation of the manuscript.

■ ABBREVIATIONS USED

CFP, cyan fluorescent protein; *c*Hep, cycloheptyl; *c*Pen, cyclopentyl; FRET, fluorescence resonance energy transfer; HAT, human African trypanosomiasis; hPDE, human phosphodiesterase; *i*Pr, isopropyl; K, kinetoplast; LLE, ligand-lipophilicity efficiency; LmjPDEB1, *Leishmania major* phosphodiesterase B1; MOE, Molecular Operating Environment; MW, microwave; N, nucleus; NECT, nifurtimox−eflornithine combination therapy; TbrPDEB1, *Trypanosoma brucei* phosphodiesterase B1; TbrPDEB2, *Trypanosoma brucei* phosphodiesterase B2; YFP, yellow fluorescent protein

■ REFERENCES

(1) Kennedy, P. G. The continuing problem of human African trypanosomiasis (sleeping sickness). *Ann. Neurol.* **2008**, *64*, 116−126.
(2) Brun, R.; Blum, J.; Chappuis, F.; Burri, C. Human African trypanosomiasis. *Lancet* **2010**, *375*, 148−159.
(3) Simarro, P. P.; Diarra, A.; Postigo, J. A. R.; Franco, J. R.; Jannin, J. G. The Human African Trypanosomiasis Control and Surveillance Programme of the World Health Organization 2000−2009: The Way Forward. *PLoS Neglected Trop. Dis.* **2011**, *5*, e1007.
(4) Fevre, E. M.; Wissmann, B. V.; Welburn, S. C.; Lutumba, P. The burden of human African trypanosomiasis. *PLoS Neglected Trop. Dis.* **2008**, *2*, e333.
(5) Yun, O.; Priotto, G.; Tong, J.; Flevaud, L.; Chappuis, F. NECT is next: implementing the new drug combination therapy for *Trypanosoma brucei gambiense* sleeping sickness. *PLoS Neglected Trop. Dis.* **2010**, *4*, e720.
(6) Ioset, J. R.; Chang, S. Drugs for Neglected Diseases *initiative* model of drug development for neglected diseases: current status and future challenges. *Future Med. Chem.* **2011**, *3*, 1361−1371.
(7) Berriman, M.; Ghedin, E.; Hertz-Fowler, C.; Blandin, G.; Renauld, H.; Bartholomeu, D. C.; Lennard, N. J.; Caler, E.; Hamlin, N. E.; Haas, B.; Bohme, U.; Hannick, L.; Aslett, M. A.; Shallom, J.; Marcello, L.; Hou, L.; Wickstead, B.; Alsmark, U. C.; Arrowsmith, C.; Atkin, R. J.; Barron, A. J.; Bringaud, F.; Brooks, K.; Carrington, M.; Cherevach, I.; Chillingworth, T. J.; Churcher, C.; Clark, L. N.; Corton, C. H.; Cronin, A.; Davies, R. M.; Doggett, J.; Djikeng, A.; Feldblyum, T.; Field, M. C.; Fraser, A.; Goodhead, I.; Hance, Z.; Harper, D.; Harris, B. R.; Hauser, H.; Hostetler, J.; Ivens, A.; Jagels, K.; Johnson, D.; Johnson, J.; Jones, K.; Kerhornou, A. X.; Koo, H.; Larke, N.; Landfear, S.; Larkin, C.; Leech, V.; Line, A.; Lord, A.; Macleod, A.; Mooney, P. J.; Moule, S.; Martin, D. M.; Morgan, G. W.; Mungall, K.; Norbertczak, H.; Ormond, D.; Pai, G.; Peacock, C. S.; Peterson, J.; Quail, M. A.; Rabbinowitsch, E.; Rajandream, M. A.; Reitter, C.; Salzberg, S. L.; Sanders, M.; Schobel, S.; Sharp, S.; Simmonds, M.; Simpson, A. J.; Tallon, L.; Turner, C. M.; Tait, A.; Tivey, A. R.; Van Aken, S.; Walker, D.; Wanless, D.; Wang, S.; White, B.; White, O.; Whitehead, S.; Woodward, J.; Wortman, J.; Adams, M. D.; Embley, T. M.; Gull, K.; Ullu, E.; Barry, J. D.; Fairlamb, A. H.; Opperdoes, F.; Barrell, B. G.; Donelson, J. E.; Hall, N.; Fraser, C. M.; Melville, S. E.; El-Sayed, N. M. The genome of the African trypanosome *Trypanosoma brucei*. *Science* **2005**, *309*, 416−422.
(8) Gould, M. K.; de Koning, H. P. Cyclic-nucleotide signalling in protozoa. *FEMS Microbiol. Rev.* **2011**, *35*, 515−541.
(9) Zoraghi, R.; Seebeck, T. The cAMP-specific phosphodiesterase TbPDE2C is an essential enzyme in bloodstream form *Trypanosoma brucei*. *Proc. Natl. Acad. Sci. U.S.A.* **2002**, *99*, 4343−4348.
(10) Seebeck, T.; Sterk, G. J.; Ke, H. M. Phosphodiesterase inhibitors as a new generation of antiprotozoan drugs: exploiting the benefit of enzymes that are highly conserved between host and parasite. *Future Med. Chem.* **2011**, *3*, 1289−1306.
(11) Oberholzer, M.; Marti, G.; Baresic, M.; Kunz, S.; Hemphill, A.; Seebeck, T. The *Trypanosoma brucei* cAMP phosphodiesterases TbrPDEB1 and TbrPDEB2: flagellar enzymes that are essential for parasite virulence. *FASEB J.* **2007**, *21*, 720−731.
(12) de Koning, H. P.; Gould, M. K.; Sterk, G. J.; Tenor, H.; Kunz, S.; Luginbuehl, E.; Seebeck, T. Pharmacological validation of *Trypanosoma brucei* phosphodiesterases as novel drug targets. *J. Infect. Dis.* **2012**, *206*, 229−237.
(13) van der Mey, M.; Hatzelmann, A.; van Klink, G. P. M.; van der Laan, I. J.; Sterk, G. J.; Thibaut, U.; Ulrich, W. R.; Timmerman, H. Novel selective PDE4 inhibitors. 2. Synthesis and structure−activity relationships of 4-aryl-substituted cis-tetra- and cis-hexahydrophthalazinones. *J. Med. Chem.* **2001**, *44*, 2523−2535.
(14) Bland, N. D.; Wang, C. H.; Tallman, C.; Gustafson, A. E.; Wang, Z.; Ashton, T. D.; Ochiana, S. O.; McAllister, G.; Cotter, K.; Fang, A. P.; Gechijian, L.; Garceau, N.; Gangurde, R.; Ortenberg, R.; Ondrechen, M. J.; Campbell, R. K.; Pollastri, M. P. Pharmacological validation of *Trypanosoma brucei* phosphodiesterases B1 and B2 as druggable targets for african sleeping sickness. *J. Med. Chem.* **2011**, *54*, 8188−8194.
(15) Ochiana, S. O.; Gustafson, A.; Bland, N. D.; Wang, C.; Russo, M. J.; Campbell, R. K.; Pollastri, M. P. Synthesis and evaluation of human phosphodiesterases (PDE) 5 inhibitor analogs as trypanosomal PDE inhibitors. Part 2. Tadalafil analogs. *Bioorg. Med. Chem. Lett.* **2012**, *22*, 2582−2584.
(16) Wang, C.; Ashton, T. D.; Gustafson, A.; Bland, N. D.; Ochiana, S. O.; Campbell, R. K.; Pollastri, M. P. Synthesis and evaluation of human phosphodiesterases (PDE) 5 inhibitor analogs as trypanosomal PDE inhibitors. Part 1. Sildenafil analogs. *Bioorg. Med. Chem. Lett.* **2012**, *22*, 2579−2581.
(17) Beghyn, T. B.; Charton, J.; Leroux, F.; Laconde, G.; Bourin, A.; Cos, P.; Maes, L.; Deprez, B. Drug to genome to drug: discovery of new antiplasmodial compounds. *J. Med. Chem.* **2011**, *54*, 3222−3240.
(18) Sircar, I.; Weishaar, R. E.; Kobylarz, D.; Moos, W. H.; Bristol, J. A. Cardiotonic agents. 7. Inhibition of separated forms of cyclic nucleotide phosphodiesterase from guinea pig cardiac muscle by 4,5-dihydro-6-[4-(1*H*-imidazol-1-yl)phenyl]-3(2*H*)-pyridazinones and related compounds. Structure−activity relationships and correlation with in vivo positive inotropic activity. *J. Med. Chem.* **1987**, *30*, 1955−1962.
(19) Edmondson, S. D.; Mastracchio, A.; He, J.; Chung, C. C.; Forrest, M. J.; Hofsess, S.; MacIntyre, E.; Metzger, J.; O'Connor, N.; Patel, K.; Tong, X.; Tota, M. R.; Van der Ploeg, L. H.; Varnerin, J. P.; Fisher, M. H.; Wyvratt, M. J.; Weber, A. E.; Parmee, E. R. Benzyl vinylogous amide substituted aryldihydropyridazinones and aryldimethylpyrazolones as potent and selective PDE3B inhibitors. *Bioorg. Med. Chem. Lett.* **2003**, *13*, 3983−3987.
(20) Schlemminger, I.; Schmidt, B.; Flockerzi, D.; Tenor, H.; Zitt, C.; Hatzelmann, A.; Marx, D.; Braun, C.; Kuelzer, R.; Heuser, A.; Kley, H.-P.; Sterk, G. J. Novel Pyrazolone-Derivatives and Their Use as PDE4 Inhibitors. 2010/05/20, 2010; Nycomed Gmbh.
(21) Wang, H.; Yan, Z.; Geng, J.; Kunz, S.; Seebeck, T.; Ke, H. Crystal structure of the *Leishmania major* phosphodiesterase LmjPDEB1 and insight into the design of the parasite-selective inhibitors. *Mol. Microbiol.* **2007**, *66*, 1029−1038.
(22) van der Mey, M.; Boss, H.; Hatzelmann, A.; van der Laan, I. J.; Sterk, G. J.; Timmerman, H. Novel selective PDE4 inhibitors. 3. In vivo antiinflammatory activity of a new series of N-substituted cis-tetra- and cis-hexahydrophthalazinones. *J. Med. Chem.* **2002**, *45*, 2520−2525.
(23) Cos, P.; Vlietinck, A. J.; Vanden Berghe, D.; Maes, L. Anti-infective potential of natural products: how to develop a stronger in vitro "proof-of-concept". *J. Ethnopharmacol.* **2006**, *106*, 290−302.
(24) Räz, B.; Iten, M.; Grether-Bühler, Y.; Kaminsky, R.; Brun, R. The Alamar Blue assay to determine drug sensitivity of African trypanosomes (*T.b. rhodesiense* and *T.b. gambiense*) in vitro. *Acta Trop.* **1997**, *68*, 139−147.
(25) Conti, M. Phosphodiesterases and cyclic nucleotide signaling in endocrine cells. *Mol. Endocrinol.* **2000**, *14*, 1317−1327.

(26) Conti, M.; Richter, W.; Mehats, C.; Livera, G.; Park, J. Y.; Jin, C. Cyclic AMP-specific PDE4 phosphodiesterases as critical components of cyclic AMP signaling. *J. Biol. Chem.* **2003**, *278*, 5493−5496.
(27) Hopkins, A. L.; Groom, C. R.; Alex, A. Ligand efficiency: a useful metric for lead selection. *Drug Discovery Today* **2004**, *9*, 430−431.
(28) Leeson, P. D.; Springthorpe, B. The influence of drug-like concepts on decision-making in medicinal chemistry. *Nat. Rev. Drug Discovery* **2007**, *6*, 881−890.
(29) Xu, R. X.; Rocque, W. J.; Lambert, M. H.; Vanderwall, D. E.; Luther, M. A.; Nolte, R. T. Crystal structures of the catalytic domain of phosphodiesterase 4B complexed with AMP, 8-Br-AMP, and rolipram. *J. Mol. Biol.* **2004**, *337*, 355−365.
(30) Zhang, K. Y. J.; Card, G. L.; Suzuki, Y.; Artis, D. R.; Fong, D.; Gillette, S.; Hsieh, D.; Neiman, J.; West, B. L.; Zhang, C.; Milburn, M. V.; Kim, S.-H.; Schlessinger, J.; Bollag, G. A glutamine switch mechanism for nucleotide selectivity by phosphodiesterases. *Mol. Cell* **2004**, *15*, 279−286.
(31) *Marvin*, version 5.6.0.4; ChemAxon: Budapest, Hungary, 2011.
(32) Calverley, P. M. A.; Sanchez-Torill, F.; McIvor, A.; Teichmann, P.; Bredenbroeker, D.; Fabbri, L. M. Effect of 1-year treatment with roflumilast in severe chronic obstructive pulmonary disease. *Am. J. Respir. Crit. Care Med.* **2007**, *176*, 154−161.
(33) Rennard, S.; Knobil, K.; Rabe, K. F.; Morris, A.; Schachter, N.; Locantore, N.; Canonica, W. G.; Zhu, Y. J.; Barnhart, F. The efficacy and safety of cilomilast in COPD. *Drugs* **2008**, *68*, 3−57.
(34) Geldern, T. v.; Harhay, M. O.; Scandale, I.; Don, R. Kinetoplastid Parasites. In *Third World Diseases*, 7th ed.; Elliott, R. L., Ed.; Springer Verlag: Berlin and Heidelberg, Germany, 2011; Vol. 7, pp 181−242.
(35) Andrade, L. O.; Andrews, N. W. The *Trypanosoma cruzi*-host-cell interplay: location, invasion, retention. *Nat. Rev. Microbiol.* **2005**, *3*, 819−823.
(36) Nwaka, S.; Ramirez, B.; Brun, R.; Maes, L.; Douglas, F.; Ridley, R. Advancing drug innovation for neglected diseases-criteria for lead progression. *PLoS Neglected Trop. Dis.* **2009**, *3*, e440.
(37) Larkin, M. A.; Blackshields, G.; Brown, N. P.; Chenna, R.; McGettigan, P. A.; McWilliam, H.; Valentin, F.; Wallace, I. M.; Wilm, A.; Lopez, R.; Thompson, J. D.; Gibson, T. J.; Higgins, D. G. Clustal W and Clustal X version 2.0. *Bioinformatics* **2007**, *23*, 2947−2948.
(38) *Molecular Operating Environment*, version 2010.10; Chemical Computing Group (CCG): Montreal, Canada, 2010.
(39) Boström, J.; Greenwood, J. R.; Gottfries, J. Assessing the performance of OMEGA with respect to retrieving bioactive conformations. *J. Mol. Graphics Modell.* **2003**, *21*, 449−462.
(40) Jones, G.; Willett, P.; Glen, R. C. Molecular recognition of receptor sites using a genetic algorithm with a description of desolvation. *J. Mol. Biol.* **1995**, *245*, 43−53.
(41) *The PyMOL Molecular Graphics System*, version 1.3; Schrödinger Inc.: New York, NY, U.S.A., 2010.
(42) Ashton, M. J.; Cook, D. C.; Fenton, G.; Karlsson, J. A.; Palfreyman, M. N.; Raeburn, D.; Ratcliffe, A. J.; Souness, J. E.; Thurairatnam, S.; Vicker, N. Selective type IV phosphodiesterase inhibitors as antiasthmatic agents. The syntheses and biological activities of 3-(cyclopentyloxy)-4-methoxybenzamides and analogues. *J. Med. Chem.* **1994**, *37*, 1696−1703.
(43) Wang, M.; Gao, M.; Mock, B. H.; Miller, K. D.; Sledge, G. W.; Hutchins, G. D.; Zheng, Q. H. Synthesis of carbon-11 labeled fluorinated 2-arylbenzothiazoles as novel potential PET cancer imaging agents. *Bioorg. Med. Chem.* **2006**, *14*, 8599−8607.
(44) Mehta, N. B.; Musso, D. L. Design and synthesis of a hapten for the radioimmunoassay of bupropion. *J. Pharm. Sci.* **1986**, *75*, 410−412.
(45) Schäfer, W.; Uhlig, G.; Zaschke, H.; Demus, D.; Diele, S.; Kresse, H.; Ernst, S.; Wedler, W. New naphthalene derivatives with liquid-crystalline glassy states. *Mol. Cryst. Liq. Cryst. Sci. Technol.* **1990**, *191*, 269−276.
(46) Thompson, W. J.; Brooker, G.; Appleman, M. M. Assay of cyclic nucleotide phosphodiesterases with radioactive substrates. *Methods Enzymol.* **1974**, *38*, 205−212.
(47) Bauer, A. C.; Schwabe, U. An improved assay of cyclic 3′,5′-nucleotide phosphodiesterases with QAE-Sephadex columns. *Naunyn Schmiedeberg's Arch. Pharmacol.* **1980**, *311*, 193−198.
(48) Hirumi, H.; Hirumi, K. Continuous cultivation of *Trypanosoma-brucei* blood stream forms in a medium containing a low concentration of serum-protein without feeder cell-layers. *J. Parasitol.* **1989**, *75*, 985−989.
(49) Berg, M.; Kohl, L.; Van der Veken, P.; Joossens, J.; Al-Salabi, M. I.; Castagna, V.; Giannese, F.; Cos, P.; Versees, W.; Steyaert, J.; Grellier, P.; Haemers, A.; Degano, M.; Maes, L.; de Koning, H. P.; Augustyns, K. Evaluation of nucleoside hydrolase inhibitors for treatment of African trypanosomiasis. *Antimicrob. Agents Chemother.* **2010**, *54*, 1900−1908.
(50) Nikolaev, V. O.; Bünemann, M.; Hein, L.; Hannawacker, A.; Lohse, M. J. Novel single chain cAMP sensors for receptor-induced signal propagation. *J. Biol. Chem.* **2004**, *279*, 37215−37218.
(51) Nikolaev, V. O.; Bünemann, M.; Schmitteckert, E.; Lohse, M. J.; Engelhardt, S. Cyclic AMP imaging in adult cardiac myocytes reveals far-reaching β_1-adrenergic but locally confined β_2-adrenergic receptor-mediated signaling. *Circ. Res.* **2006**, *99*, 1084−1091.
(52) Gloerich, M.; Bos, J. L. Epac: defining a new mechanism for cAMP action. *Annu. Rev. Pharmacol. Toxicol.* **2010**, *50*, 355−375.
(53) Furger, A.; Jungi, T. W.; Salomone, J. Y.; Weynants, V.; Roditi, I. Stable expression of biologically active recombinant bovine interleukin-4 in *Trypanosoma brucei*. *FEBS Lett.* **2001**, *508*, 90−94.
(54) Cross, G. A. M.; Manning, J. C. Cultivation of *Trypanosoma brucei* sspp. in semi-defined media. *Parasitology* **1973**, *67*, 315−331.
(55) Brun, R.; Schonenberger, M. Cultivation and in vitro cloning of procyclic culture forms of *Trypanosoma brucei* in a semi-defined medium. *Acta Trop.* **1979**, *36*, 289−292.

NOTE ADDED AFTER ASAP PUBLICATION

This paper was published online October 8, 2012. Erroneous residue numbers were corrected throughout, and the corrected version was reposted October 17, 2012.